Journal of Computational Physics **167,** 39–71 (2001)
doi:10.1006/jcph.2000.6656, available online at http://www.idealibrary.com on IDEAL®

Three-Dimensional Vortex Methods for Particle-Laden Flows with Two-Way Coupling

J. H. Walther* and P. Koumoutsakos*,†

**Institute of Computational Sciences, ETH Zürich, CH-8092 Zürich, Switzerland;*
and †CTR, NASA Ames 202A-1, Moffett Field, California 94035
E-mail: walther@inf.ethz.ch; petros@inf.ethz.ch

Received May 3, 2000; revised September 29, 2000

This paper presents a three-dimensional viscous vortex method for the simulation of particulate flows with two-way coupling. The flow is computed using Lagrangian vortex elements advected with the local velocity, while their strength is modified to account for viscous diffusion, vortex stretching, and generating vorticity induced by the particles. The solid particles move according to viscous drag and gravity, creating vorticity, which is discretised using vortex elements. This method adaptively tracks the evolution of the vorticity field and the generation of new computational elements to account for the vorticity source term. A key aspect of the present scheme is the re-meshing of the computational elements to adaptively accommodate the production of vorticity induced by the solid particles, and to ensure sufficient support for the proper resolution of the diffusion equation. High-order moment-conserving formulas are implemented to maintain the adaptive character of the method while they remain local to minimize the computational cost. These formulas are also implemented in the particle–mesh interpolation of the field and particle quantities in the context of a Vortex-in-Cell algorithm. The method is validated against the results of a related finite-difference study for an axisymmetric swirling flow with particles. The method is then applied to the study of a three-dimensional particle blob falling under the effect of gravity. It is shown that drastically different behaviours are found depending on the presence of an initial vorticity field.

Key Words: vortex methods; particle-laden flows; Lagrangian method.

1. INTRODUCTION

The frequent occurrence of particle-laden flows in nature and industry has made this field an active area of research in the last decades. The physical problems range from environmental particulate pollution problems [24] to particulate flows in fluidised bed reactors, particle generation and reaction processes, and solids transport and separation [16].

0021-9991/01 $35.00

Traditionally, a *one-way* coupling between the phases has been employed for *dilute* systems, but the preferential accumulation of solid particles in regions of high fluid strain rate and low vorticity [18] can result in high values of the local particle concentration, indicating the presence of a significant (local) coupling of the two phases. Thus, even in nominally dilute systems, it is desirable that the numerical method allows a *two-way* transfer of momentum between the particulate and fluid phases. In simulations of particulate flows with two-way coupling the solid particles are advanced by solving Newton's law of motion with forces that account for the hydrodynamic interaction with the flow field (e.g., Stokes drag, buoyancy, added mass, etc.). At the same time, their motion imparts vorticity onto the neighbouring fluid elements. The proper generation of vorticity (and accordingly the complete *two-way* coupling) for each solid particle would involve the solution of the Navier–Stokes equation around each particle [21], which for very large number of particles is presently a computationally intractable task. Alternatively, the generation of vorticity induced by the solid particles can be modelled to enforce momentum conservation with the model forces induced on the solid particles by the fluid flow.

A key aspect of the simulation of particle-laden flows is the interpolation of flow quantities between the solid particles and the computational elements. These computational elements may be Eulerian as in finite-difference and spectral element methods [20] or Lagrangian, as the vortex elements used in the present study. The governing flow equations are solved for these elements by taking into account the particle forcing in terms of vorticity generation. In turn, fluid velocity is interpolated from the computational elements onto the solid particles to determine the hydrodynamic forces.

Simulations of particle-laden flows using particle (vortex) methods offer an interesting alternative to grid-based methods due to their inherent adaptivity and the minimal amount of numerical dissipation associated with the discretisation of the non-linear convection term. Efficient computations are possible by using fast multipole algorithms for flows in unbounded domains and hybrid algorithms (such as particle–mesh) for unbounded and periodic domains. However, issues such as the distortion of the computational particles and the interpolation of particle quantities onto the Lagrangian computational elements has not been extensively addressed in the past; in particular, in the context of three-dimensional simulations. In this paper it is shown that these issues can be accurately resolved by implementing effective re-meshing formulas.

We consider flows in periodic domains and the present work extends the Vortex-in-Cell (VIC) algorithm originally proposed for the study of plasma by Birdsall and Fuss [4], and later applied to fluid flow problems by Christiansen [12] to the study of three-dimensional, two-phase particulate viscous flows with a two-way coupling of the phases.

A key aspect for the convergence of vortex methods is the enforcement of the particle overlap throughout the evolution of the flow field. We ensure the accuracy of the method and the accurate treatment of the two-way coupling by applying a re-meshing strategy of the vortex elements, allowing these to be created where the vorticity source term is non-negligible. The re-meshing also secures a proper discretisation of the diffusion which is computed using the Particle Strength Exchange (PSE) scheme by Degond and Mas-Gallic [17]. The forces acting on the solid particles include viscous drag, but implementation of additional forces (e.g., added mass and lift forces) [33] is straightforward.

Particle (vortex) methods have been applied to a number of studies of particulate flows including two-dimensional studies of Rayleigh–Taylor instability [1, 25, 49, 51, 52], mixing

layers [7, 8, 32], and of wakes [46]. Three-dimensional simulations include the work of Brecht and Ferrante [5, 6] for studies of inviscid buoyant bubbles.

Recently, Chen and Marshall [8] proposed a two-dimensional particle (vortex) method for particulate flows with two-way coupling. The coupling was achieved through a vorticity source term, and the (vortex) particle support by a particle creation scheme. In the context of particle (vortex) methods, the present study is one of the first studies to consider three-dimensional, viscous, particulate flow.

The present algorithm is validated by considering the particle laden flow in an inviscid, two-dimensional vortex patch. The results are compared with high-resolution finite-difference solutions [8] and the convergence is studied by varying the numerical parameters of the problem. Next, we consider the three-dimensional simulation of an initially spherical suspension of solid particles falling due to gravity in a viscous fluid. This case demonstrates the adaptivity of the algorithm and the solution is compared qualitatively with a drop falling in a viscous fluid [34, 48, 47].

The remaining part of the paper is organised as follows: Section 2 outlines the governing equations, and Section 3 the numerical method. The results are presented in Section 4, and summarised in Section 5.

2. GOVERNING EQUATIONS

We consider simulations of three-dimensional particle-laden flows. In our treatment we employ the following approximations: (i) the particles consist of rigid spheres of the same diameter, (ii) the particle forces are limited to fluid drag and gravity forces, (iii) particle collision is not taken into account, and (iv) the flow is periodic and incompressible. With these assumptions, the equations governing the motion of the solid particles and the fluid elements are described as follows.

2.1. *Fluid Motion*

The governing equation for an incompressible fluid with constant kinematic viscosity (ν) may be given in terms of the vorticity transport equation

$$\frac{D\boldsymbol{\omega}}{Dt} = (\boldsymbol{\omega}\cdot\boldsymbol{\nabla})\boldsymbol{v} + \nu\boldsymbol{\nabla}^2\boldsymbol{\omega} + \phi, \tag{1}$$

where $\boldsymbol{v}$ is the velocity, $\boldsymbol{\omega} = \boldsymbol{\nabla}\times\boldsymbol{v}$ the fluid vorticity, and $D/Dt = \partial/\partial t + \boldsymbol{v}\cdot\boldsymbol{\nabla}$ the material derivative. The vorticity source term (ϕ) is expressed as

$$\phi = \frac{1}{\rho}\boldsymbol{\nabla}\times\boldsymbol{f}, \tag{2}$$

where $\boldsymbol{f}$ is the body force per unit volume, and ρ the fluid density.

The fluid velocity can be recovered from the vorticity through a Poisson equation with the aid of a solenoidal vector potential, $\boldsymbol{\Psi}$ (such that $\boldsymbol{v} = \boldsymbol{\nabla}\times\boldsymbol{\Psi}$),

$$\boldsymbol{\nabla}^2\boldsymbol{\Psi} = -\boldsymbol{\omega}. \tag{3}$$

In this study we conduct simulations in a domain periodic in all three space dimensions with length L so that $\boldsymbol{\Psi}(x) = \boldsymbol{\Psi}(x + L)$.

2.2. *Solid Particle Motion*

In the following the solid particle quantities are denoted by the subscript p, while quantities pertaining to the fluid do not have a subscript.

The solid particles are considered as rigid spheres with diameter (d_p) and density (ρ_p). Their motion is described by their instantaneous position ($\boldsymbol{x}_p$) and velocity ($\boldsymbol{u}_p$) and is governed by Newton's law,

$$\begin{aligned} \frac{\mathrm{d}\boldsymbol{x}_p}{\mathrm{d}t} &= \boldsymbol{u}_p, \\ \rho_p \mathrm{vol}_p \frac{\mathrm{d}\boldsymbol{u}_p}{\mathrm{d}t} &= \boldsymbol{f}_p, \end{aligned} \tag{4}$$

where $p = 1, \ldots, N_p$, $\mathrm{vol}_p = \pi d_p^3/6$ is the volume of the particle, and $\boldsymbol{f}_p$ is the total force acting on the particle. In the present paper we have limited the number of forces to include viscous drag force $\boldsymbol{f}_d$ and gravity $\boldsymbol{f}_g$. However, the inclusion of additional forces (e.g., added mass, pressure forces) is straightforward. Thus,

$$\boldsymbol{f}_p = \boldsymbol{f}_d + \boldsymbol{f}_g. \tag{5}$$

The viscous drag force induced by the flow on the solid particles is described as [37]

$$\boldsymbol{f}_d = \frac{1}{2}\rho C_d \frac{\pi}{4} d_p^2 (\boldsymbol{v}(\boldsymbol{x}_p) - \boldsymbol{u}_p)|\boldsymbol{v}(\boldsymbol{x}_p) - \boldsymbol{u}_p|, \tag{6}$$

where $\boldsymbol{v}(\boldsymbol{x}_p)$ is the fluid velocity at the position of the particle, C_d is the drag coefficient,

$$C_d = \begin{cases} \frac{24}{\mathrm{Re}_p}\left(1 + 0.15\mathrm{Re}_p^{0.687}\right), & \mathrm{Re}_p < 1000, \\ 0.44, & \mathrm{Re}_p > 1000, \end{cases} \tag{7}$$

and Re_p is the particle Reynolds number,

$$\mathrm{Re}_p = \frac{|\boldsymbol{u}_p - \boldsymbol{v}(\boldsymbol{x}_p)|d_p}{\nu}. \tag{8}$$

The particles are furthermore subjected to a gravity force

$$\boldsymbol{f}_g = \mathrm{vol}_p(\rho_p - \rho)\boldsymbol{g}, \tag{9}$$

where $\boldsymbol{g}$ is the acceleration due to gravity.

The source term in Eq. (2) models the creation of vorticity from the solid surfaces of the particles. This vorticity source is in general proportional to the pressure gradient and the tangential acceleration of the surface of the particle and accounted for here by a model drag force; thus $\boldsymbol{f} = \boldsymbol{f}_d$. The hydrostatic pressure forces ($-\mathrm{vol}_p\rho\boldsymbol{g}$) are accounted for without directly producing any vorticity.

3. VORTEX PARTICLE METHOD

3.1. *Fluid Motion*

We discretise the governing Navier–Stokes equations in $\boldsymbol{v}$–$\boldsymbol{\omega}$ form (Eq. (1)) using a vortex particle method. The vorticity field is discretised using N Lagrangian (vortex) particles,

$$\boldsymbol{\omega}(\boldsymbol{x}) = \sum_{i=1}^{N} \boldsymbol{\alpha}_i \eta_\sigma(\boldsymbol{x} - \boldsymbol{x}_i), \tag{10}$$

$$\boldsymbol{\alpha}_i = \mathrm{vol}_i \boldsymbol{\omega}(\boldsymbol{x}_i), \tag{11}$$

where $(\boldsymbol{x}_i)$ and $(\boldsymbol{\alpha}_i)$ denote the location and strength of the vortex particle, respectively. The vorticity field of each particle is mollified over a support of size σ by a smooth function $\eta_\sigma(\boldsymbol{x})$. Typical examples of such functions are radially symmetric Gaussians usually used in pure Lagrangian methods or tensorial products of polynomials or splines in hybrid particle–mesh methods. The order of the approximation is proportional to the number of moments shared by the smoothing function and the Dirac delta-function (cf. [3, 22]).

The vortex particles are advected using a fractional two-step algorithm. During the first, inviscid step, the particle locations are modified to account for convection while the particle strengths are changed to account for vortex stretching,

$$\frac{\mathrm{d}\boldsymbol{x}_i}{\mathrm{d}t} = \boldsymbol{v}(\boldsymbol{x}_i), \tag{12}$$

$$\frac{\mathrm{d}\boldsymbol{\alpha}_i}{\mathrm{d}t} = \mathrm{vol}_i (\boldsymbol{\omega}(\boldsymbol{x}_i) \cdot \boldsymbol{\nabla}) \boldsymbol{v}(\boldsymbol{x}_i), \tag{13}$$

where $i = 1, \ldots, N$. In the present computations, we use the conservative from $(\boldsymbol{\nabla} \cdot (\boldsymbol{\omega} : \boldsymbol{v}))$.

The inviscid step is followed by a second viscous step accounting for the effects of diffusion and vorticity generation in the fluid elements induced by the solid particles. During this step the vortex particles are considered "frozen" in their locations while their strength is modified to account for the effects of diffusion

$$\frac{\mathrm{d}\boldsymbol{x}_i}{\mathrm{d}t} = 0, \tag{14}$$

$$\frac{\mathrm{d}\boldsymbol{\alpha}_i}{\mathrm{d}t} = \mathrm{vol}_i (\nu \boldsymbol{\nabla}^2 \boldsymbol{\omega}(\boldsymbol{x}_i) + \boldsymbol{\phi}(\boldsymbol{x}_i)), \tag{15}$$

and $i = 1, \ldots, N$. Using this Lagrangian algorithm the vortex elements automatically adapt to areas of the flow field where vorticity is being generated by the motion of the solid particles.

3.2. *Diffusion*

Particle methods are well suited to the discretisation of problems described by an integral operator. The integral operator can be discretised using as quadrature points the location of the particles which are not required to occupy regular grid locations. In order to handle the diffusion operator in the context of particle methods the key idea is then to replace the Laplacian with an equivalent integral operator. The links between integral and diffusion operators have long been exploited in the field of kinetic equations, but in general in

the other direction, namely, to derive a diffusion approximation of integral operators that model particle collisions [40]. The Particle Strength Exchange (PSE) method introduced by Degond and Mas-Gallic [17] replaces the Laplacian by an integral operator as

$$\nabla^2\boldsymbol{\omega}(\boldsymbol{x}) \approx \nabla^2_\sigma\boldsymbol{\omega}(\mathbf{x}) = \sigma^{-2}\int[\boldsymbol{\omega}(\mathbf{y}) - \boldsymbol{\omega}(\mathbf{x})]\zeta_\sigma(\mathbf{y}-\mathbf{x})\,\mathrm{d}\mathbf{y}. \tag{16a}$$

The accuracy of this approximation is related to the moment properties of ζ_σ. For a method of order m the kernel $\zeta_\sigma(\boldsymbol{x}) = \sigma^{-3}\zeta(\boldsymbol{x}/\sigma)$ is the mth order diffusion kernel satisfying the moment conditions

$$\begin{aligned}
&\iiint \boldsymbol{x}^{\boldsymbol{\alpha}}\zeta(\boldsymbol{x})\,\mathrm{d}V = 2, && \text{if } \boldsymbol{\alpha} = 2\boldsymbol{e}_i \;\; i \in \{1,2,3\},\ 1 \le |\boldsymbol{\alpha}| \le m+1,\\
&\iiint \boldsymbol{x}^{\boldsymbol{\alpha}}\zeta(\boldsymbol{x})\,\mathrm{d}V = 0, && \text{if } \boldsymbol{\alpha} \ne \boldsymbol{e}_i \quad i \in \{1,2,3\},\\
&\iiint |\boldsymbol{x}|^{m+2}|\zeta(\boldsymbol{x})|\,\mathrm{d}V < \infty.
\end{aligned} \tag{16b}$$

Here $\boldsymbol{\alpha} = (\alpha_1, \alpha_2, \alpha_3) \in N^3$, $\boldsymbol{x}^{\boldsymbol{\alpha}} \equiv \prod_{i=1}^3 \boldsymbol{x}_i^{\alpha_i}$, $|\boldsymbol{\alpha}| = \sum_{i=1}^3 \alpha_i$, and $\boldsymbol{e}_i$ are the unit vectors (1, 0, 0), (0, 1, 0), and (0, 0, 1), respectively; cf. [17].

The second-order kernel proposed by Cottet [14] is used (Fig. 1):

$$\zeta(\boldsymbol{x}) = \frac{15}{\pi^2}\frac{1}{|\boldsymbol{x}|^{10}+1}. \tag{17}$$

When the integral operator is discretised we obtain an algorithm for the update of the particle (vortex) strengths as

$$\frac{\mathrm{d}\boldsymbol{\alpha}_i}{\mathrm{d}t} = \frac{\nu}{\sigma^2}\sum_j \zeta_\sigma(\boldsymbol{x}_i - \boldsymbol{x}_j)(\mathrm{vol}_i\boldsymbol{\alpha}_j - \mathrm{vol}_j\boldsymbol{\alpha}_i). \tag{18}$$

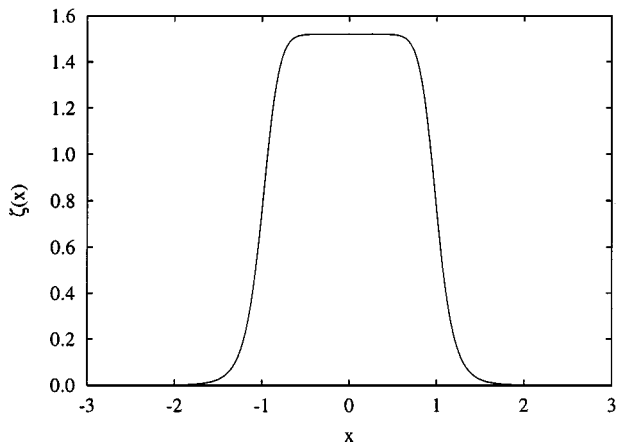

FIG. 1. Second-order diffusion kernel used in the particle strength exchange scheme.

3.3. *Vortex-in-Cell*

The computationally intensive part of particle (vortex) methods is the calculation of the velocity field, as each particle induces a velocity field on all other particles. The classical cost of the method scales as $\mathcal{O}(N^2)$ but it can be reduced to $\mathcal{O}(N)$ or $\mathcal{O}(N \log N)$ using fast multipole methods [9] or particle–mesh techniques [23]. Particle–mesh techniques are in general faster as they take advantage of the availability of fast Fourier transforms for the solution of Poisson's equation. They have the drawback that they require the presence of a grid for the evaluation of the velocity. However, it should be emphasized that particle methods require in general a periodic projection of the flow field carried by the particles onto a set of overlapping particles. The projection onto a regular mesh uses a high-order interpolation formula [15] that would be difficult to construct for mesh-free particle methods, cf. [26, 31]. The accurate interpolation of particle–grid quantities is a subject of ongoing investigation [42] and is further addressed in Section 3.5 of this paper.

The present study employs the particle–mesh technique using $(N_x \times N_y \times N_z)$ grid points with an equidistant mesh spacing (h). At each time step the vorticity field is constructed on the mesh from the particle (vortex) strength using high-order assignment functions (see Section 3.4). The vector Poisson equation (Eq. (3)) is discretised using second-order finite differences and solved subject to periodic boundary conditions using fast Fourier transforms [43]. The velocity field and the vorticity stretching are computed on the mesh using fourth-order finite differences and interpolated back onto the vortex particles to update their position and strength. Second-order finite differences were also tested but were found to produce a less solenoidal vorticity field than the fourth-order scheme.

3.4. *Particle–Mesh Interpolation*

A key aspect of particle–mesh techniques is the accurate and efficient assignment of particle values to the mesh and the interpolation of the field quantities from the mesh to the particles. Only these particle field variations with wavelengths longer than those described by the mesh-spacing can be accurately represented by the respective mesh values. The finite grid size produces a loss of information which may be viewed as an aliasing error [15].

The assignment of the mesh vorticity from the particle strength and the interpolation of the particle values from the mesh use the moment-conserving M_4' scheme proposed by Monaghan [35] for one-dimensional smooth particle hydrodynamics and later applied to two- and three-dimensional vortex methods by Cottet and Koumoutsakos [15]. These moment-conserving interpolation kernels reduce the effects of aliasing without being impractical and they have compact support, that very closely approximates the ideal low-pass filter sinc (x). The moment-conserving B-splines $\mathcal{S}_n$ possesses both properties and have been shown to introduce minimal numerical dissipation in simulations using vortex methods [15]. They are continuous up to the $n-1$ derivative and therefore their Fourier transform decays as $-k^{-n}$. Their effectiveness in eliminating the effect of aliasing as a function of the wave number k and the grid wave number $k_g = 2\pi/\Delta x$ is expressed as $|1 - mk_g/k|^{-n}$ [23]. High-order interpolation kernels can be constructed efficiently using a recursive formulation as described by Sagredo *et al.* [42]. The interpolation formula in three dimensions consists of a tensorial product of its one-dimensional counterparts and it can be expressed as

$$\mathbf{\Gamma}_j = \sum_i \mathbf{\Gamma}_i W\left(\frac{x_j - x_i}{h}\right) W\left(\frac{y_j - y_i}{h}\right) W\left(\frac{z_j - z_i}{h}\right), \tag{19}$$

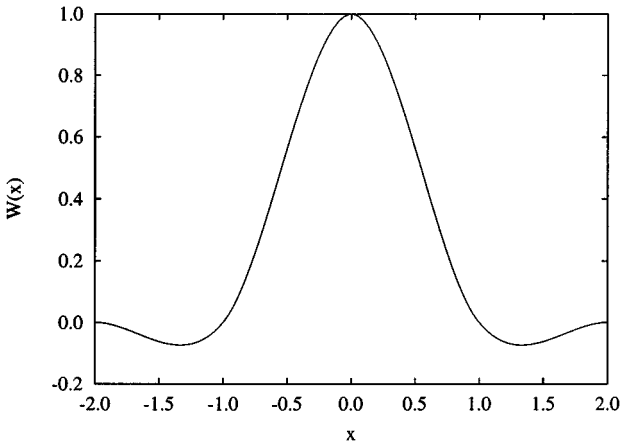

FIG. 2. M_4' interpolation kernel for assignment and interpolation.

where $W(x)$ is the M_4' interpolation kernel

$$W(x) = \begin{cases} 1 - \frac{5}{2}|x|^2 + \frac{3}{2}|x|^3, & |x| < 1, \\ \frac{1}{2}(2 - |x|)^2(1 - |x|), & 1 < |x| < 2, \\ 0, & |x| > 2. \end{cases} \tag{20}$$

cf. Fig. 2, and $(\mathbf{\Gamma}_j, \boldsymbol{x}_j)$ and $(\mathbf{\Gamma}_j, \boldsymbol{x}_i)$ are the mesh and particle values, respectively (and vice versa). Thus, in three dimensions a particle will assign values to the nearest 64 grid points, and conversely interpolation involves the 64 nearest grid points.

The M_4' scheme conserves the first three moments of the interpolant, in particular the vorticity moments $(\mathbf{\Omega}_i)$.

$$\begin{aligned} \mathbf{\Omega}_0 &= \int\int\int \boldsymbol{\omega}\, \mathrm{d}V, \\ \mathbf{\Omega}_1 &= \frac{1}{2} \int\int\int \boldsymbol{x} \times \boldsymbol{\omega}\, \mathrm{d}V, \\ \mathbf{\Omega}_2 &= \frac{1}{3} \int\int\int \boldsymbol{x} \times (\boldsymbol{x} \times \boldsymbol{\omega})\, \mathrm{d}V. \end{aligned} \tag{21}$$

From a computational point of view, the interpolation can be implemented efficiently for both vector and parallel computer architectures, since the field value at each particle can be interpolated independently. This is generally not true for the assignment procedure where grid points will receive contributions from more than one particle. In the present study with approximately one vortex particle per grid point, sorting the vortex particles in a cell index list and adding the particle contributions from the particles in the surrounding $(4 \times 4 \times 4)$ cells results in short and inefficient loops. Instead, during the re-meshing procedure (see below) the vortex particles are numbered according to their positions on the mesh in increments larger than 4 (for the M_4' scheme) in each spatial direction, cf. Fig. 3. This secures that vortex particles stored consecutively in memory will assign their strength to different subsets of the mesh, hence allowing vectorisation. The assignment procedure is subsequently split into pieces of vectorisable loops. For vector-parallel execution, the vectorised loop is

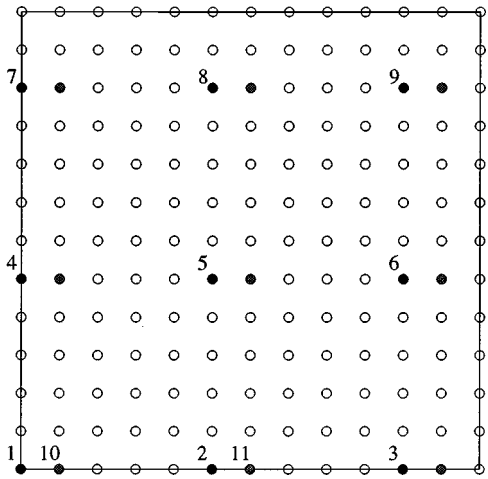

FIG. 3. During the re-meshing the new vortex particles are created on the mesh in increments larger than four in each spatial direction to allow vectorisation of the assignment procedure. The sketch shows a two-dimensional example of the particle mesh and the numbering of the first 11 particles after re-meshing.

furthermore split into pieces, an inner and outer loop, which allows parallelisation of the outer and vectorisation of the inner loop, respectively.

3.5. *Vortex Particle Re-meshing*

Lagrangian numerical methods enjoy automatic adaptivity and the elimination of the need to discretise explicitly the non-linear convection term but at the same time it is necessary to address the "grid" distortion induced by the flow map and to handle efficiently the resolution of viscous effects on the particle (vortex) locations. This can be handled by a re-meshing of the flow field. During re-meshing the particle strength is assigned to the mesh according to Eq. (19) and the (vortex) particles are replaced by a new set of particles released from the grid points where the mesh vorticity is non-negligible (i.e., where $|\boldsymbol{\omega}|/|\boldsymbol{\omega}_{\max}| > \epsilon$, and $\epsilon \ll 1$). The strength of the new particles is calculated using the formulas used for particle-mesh interpolation (Eq. (19)); see Fig. 2. Thus, the present re-meshing scheme is conservative ($\mathrm{d}\boldsymbol{\Omega}_0/\mathrm{d}t = 0$) and avoids spurious fluid forcing, since the force and torque acting on the fluid are proportional to the rate-of-change of $\boldsymbol{\Omega}_1$ and $\boldsymbol{\Omega}_2$, respectively. Specifically, for unbounded flows the fluid force ($\boldsymbol{F}$) is given by [41]

$$\boldsymbol{F} = -\rho \frac{\mathrm{d}\boldsymbol{\Omega}_1}{\mathrm{d}t}. \tag{22}$$

Re-meshing may be viewed as a method for introducing sub-grid scaling in vortex methods to eliminate the spurious structures that are introduced by the (vortex) particle distortion. In that sense re-meshing may be viewed as an effective way of introducing sub-grid scale modeling to vortex methods and could serve as an alternative approach to the method of hairpin removal [11, 19] and the use of Lagrangian anisotropic sub-grid scale models [13, 28]. The need for re-meshing in vortex particle methods was demonstrated by Knio and Ghoniem [26] and Koumoutsakos [27] for studies of two- and three-dimensional inviscid flow problems. Re-meshing is also a key aspect of the simulation of diffusion using the method of particle strength exchange. As the support of the vorticity increases by diffusion the PSE scheme requires the presence of "ghost" particles to effectuate this increase of the vorticity support.

Additionally, in the case of particle laden flow re-meshing is utilized to ensure the generation of vortex particles in the regions of the flow where the rotational part of the forcing from the solid particle is non-zero and fluid vorticity is created according to Eq. (2). The frequency of re-meshing can be determined by monitoring the particle overlap and acting when a certain threshold is exceeded. However for the flows under consideration diagnostics such as linear and angular impulse did not differ by more than 5% from cases where re-meshing was employed after every time step. Thus, re-meshing is currently performed at the end of each time step to allow efficient identification of neighbouring (vortex) particles during the diffusion procedure for the particle strength exchange scheme and to secure an optimal support of the vorticity field.

3.6. *Solid Particle Motion*

The forces on the solid particles given by Eqs. (6)–(9) are computed by interpolating the fluid velocity obtained on the mesh onto the solid particles using the M_4' scheme (Eq. (19))

$$\boldsymbol{v}(\boldsymbol{x}_p) = \sum_m \boldsymbol{v}_m W(\boldsymbol{x}_p - \boldsymbol{x}_m). \tag{23}$$

The position and velocity are updated according to Eq. (4) using the second-order leapfrog scheme

$$\boldsymbol{u}_p^{n+\frac{1}{2}} = \boldsymbol{u}_p^{n-\frac{1}{2}} + \delta t \frac{\boldsymbol{f}_p^n}{\rho_p \mathrm{vol}_p}, \tag{24}$$

$$\boldsymbol{x}_p^{n+1} = \boldsymbol{x}_p^n + \delta t \boldsymbol{u}_p^{n+\frac{1}{2}}, \tag{25}$$

and where the superscript (n) indicates the time step.

The velocity of the solid particles at time step (n) required in the calculation of $\boldsymbol{f}_p^n$ (cf. Eq. (6)) is approximated by the velocity at $(n - \frac{1}{2})$, or computed by iteration

$$\boldsymbol{u}_p^n \approx \frac{1}{2}\left(\tilde{\boldsymbol{u}}_p^{n+\frac{1}{2}} + \boldsymbol{u}_p^{n-\frac{1}{2}}\right), \tag{26}$$

where $\tilde{\boldsymbol{u}}_p^{n+\frac{1}{2}}$ is the most recent value of $\boldsymbol{u}_p$ at time $(n + \frac{1}{2})$ computed by iteration of Eqs. (6), (26), and (24), respectively. The leapfrog scheme offers in the present study a reasonable compromise between accuracy, storage requirements, and stability. Furthermore, the time-symmetry secures conservation of energy [23].

3.7. *Two-Way Coupling*

The two-way coupling is achieved in conjunction with the vortex particle re-meshing and the computation of diffusion. The force imparted by the solid particles onto the fluid elements is interpolated onto the mesh and is differentiated to obtain the vorticity source term. The algorithm proceeds with the following steps. After the calculation of the inviscid step (Eqs. (12) and (13)):

1. Assign the mesh vorticity from the N vortex particles using Eq. (19)

$$\boldsymbol{\omega}(\boldsymbol{x}_m) = \frac{1}{h^3} \sum_i^N \boldsymbol{\alpha}_i W(\boldsymbol{x}_m - \boldsymbol{x}_i).$$

2. Assign the mesh source term from the fluid forces acting on the N_p solid particles

$$\boldsymbol{f}(\boldsymbol{x}_m) = -\sum_{p}^{N_p} \boldsymbol{f}_d W(\boldsymbol{x}_m - \boldsymbol{x}_p).$$

3. Compute diffusion on the mesh using the particle strength exchange (Eq. (18)) where (h) is the smoothing length scale (σ).
4. Compute the vorticity source term $(\boldsymbol{\nabla}^h \times (\boldsymbol{f}/\rho))$ and update the mesh vorticity.
5. "Re-initialize" vortex particles at the mesh points where the vorticity is non-negligible.

By applying the same interpolation kernel for the interpolation of the fluid velocity onto the solid particles and for the assignment of the forces on the solid particles onto the fluid elements, the conservation of total kinetic energy balance of the system is enforced; cf. Sundaram and Collins [44]. Also, since the interpolation kernel satisfies $\sum_q W(x - x_q) = 1$, the exchange of momentum between the two phases is conservative [44]. The conservation of momentum is demonstrated in the three-dimensional test case presented in Section 4.2.

3.8. *Algorithm Summary*

To summarise, the present three-dimensional particle (vortex) algorithm for particle-laden flows with two-way coupling proceeds as follows. Given the initial vorticity field and volume of the vortex particles, we calculate the initial particle strength according to $\boldsymbol{\alpha}_i^0 = \mathrm{vol}_i \boldsymbol{\omega}(\boldsymbol{x}_i^0)$.

1. Inviscid step:
   (i) Assign the mesh vorticity from the vortex particles:

$$\boldsymbol{\omega}(\boldsymbol{x}_m) = \frac{1}{h^3} \sum_{i}^{N} \boldsymbol{\alpha}_i W(\boldsymbol{x}_m - \boldsymbol{x}_i).$$

   (ii) Solve the Poisson equation for the vector potential $(\boldsymbol{\nabla}^2 \boldsymbol{\Psi} = -\boldsymbol{\omega})$.
   (iii) Compute the fluid velocity from the vector potential $(\boldsymbol{v} = \boldsymbol{\nabla}^h \times \boldsymbol{\Psi})$.
   (iv) Compute the vorticity stretching term $(\boldsymbol{\nabla}^h \cdot (\boldsymbol{\omega} : \boldsymbol{v}))$.
   (v) Compute the forces on the solid particles in the first step of the Runge–Kutta cycle:
      a. Interpolate the fluid velocity to the position of the solid particles:

$$\boldsymbol{v}(\boldsymbol{x}_p) = \sum_{m} \boldsymbol{v}_m W(\boldsymbol{x}_p - \boldsymbol{x}_m).$$

      b. Compute the fluid forces on the solid particles using Eqs. (6)–(9).
      c. Update the velocity and position of the solid particles according to Eqs. (24) and (25).
      d. Enforce periodic boundary conditions for the solid particles.
   (vi) Interpolate the velocity to the vortex particles:

$$\boldsymbol{v}_i = \sum_{m} \boldsymbol{v}_m W(\boldsymbol{x}_m - \boldsymbol{x}_i).$$

(vii) Interpolate the stretching to the vortex particles:

$$(\boldsymbol{\alpha}_i \cdot \nabla)\boldsymbol{v}_i = h^3 \sum_m \nabla^h \cdot (\boldsymbol{\omega} : \boldsymbol{v}) W(\boldsymbol{x}_m - \boldsymbol{x}_i).$$

(viii) Update the position and strength of the vortex particles (Eqs. (12) and (13)).

(ix) Enforce periodic boundary conditions for the vortex particles.

2. Viscous step (compute the influence from the diffusion and the source term): See Section 3.7.

3. Return to Step 1.

The inviscid step is solved using low-storage, third-order Runge–Kutta time integration [50]; thus Step (1) is repeated accordingly. Step (v) is only invoked during the first step of the Runge–Kutta cycle.

4. RESULTS

In the following, we present validation studies of particle laden flows in a two-dimensional inviscid vortex patch for which one-dimensional high resolution finite difference solution exists [8].

Next, we consider the three-dimensional flow that develops from an initially spherical suspension of particles falling due to gravity in an quiescent fluid. The phenomena observed display a remarkable resemblance to that of a drop falling in a viscous fluid; cf. Thomson and Newall [48].

4.1. *Validation Study: Gaussian Patch*

The dynamic behaviour of a suspension of particles in a two-dimensional inviscid vortex patch is simulated, applying the present method in a "two-dimensional" mode by using four grid points in the direction normal to the plane of the patch and neglecting the vorticity-stretching term. The influence of the grid resolution (N_g), the number of particles (N_p), and the time step (δt) is studied by performing a systematic refinement of these parameters. The different cases are listed in Table 1, where N_p is the total number of solid particles used

TABLE 1
Numerical Parameters Used in the Study of a Suspension in a Two-Dimensional Vortex Patch

Case	N_p	N_g	δt
1	10^4	128×128	0.1
2	10^5	128×128	0.1
3	10^3	128×128	0.1
4	10^4	64×64	0.1
5	10^5	64×64	0.1
6	10^4	64×64	0.2
7	10^4	256×256	0.1

Note. N_p is the total number of particles used in the three-dimensional method and corresponds to $N_p/4$ for the two-dimensional case. N_g is the number of grid points, and δt the non-dimensional time step.

and hence corresponds to $N_p/4$ particles in two dimensions. The results are compared with the two-dimensional finite-difference and vortex method results of Chen and Marshall [8].

Following [8] the initial vorticity ($\omega(r)$) and concentration ($c(r)$) fields are truncated Gaussians; i.e., $\omega(r) = \omega_0 \exp(-r^2/r_0^2)$, and $c(r) = c_0 \exp(-r^2/r_0^2)$ for $r < 2.5r_0$ and zero elsewhere, where r_0 is the initial radius of the vortex patch. The results are non-dimensionalised using r_0, and the total circulation $\Gamma = \omega_0 \pi r_0^2 (1 - e^{-(2.5)^2})$.

The initial vorticity field is discretised using vortex particles on the VIC mesh. The initial position of the solid particles is given by a two-dimensional normal distribution with zero mean and variance $r_0^2/2$, and a uniform random distribution in the third direction. The initial particle velocity equals the fluid velocity.

The flow is solved subject to a periodic boundary condition in all spatial direction and to avoid significant influence from the mirror vortex patches the size of the computational domain (L) is chosen sufficiently large (here $L = 20r_0$). The radial vorticity and concentration profiles are averaged in the circumferential direction using simple binning.

The vorticity and concentration profiles obtained with the present method for a mesh resolution of 256^2 and using 10^4 solid particles are compared in Fig. 4 with the

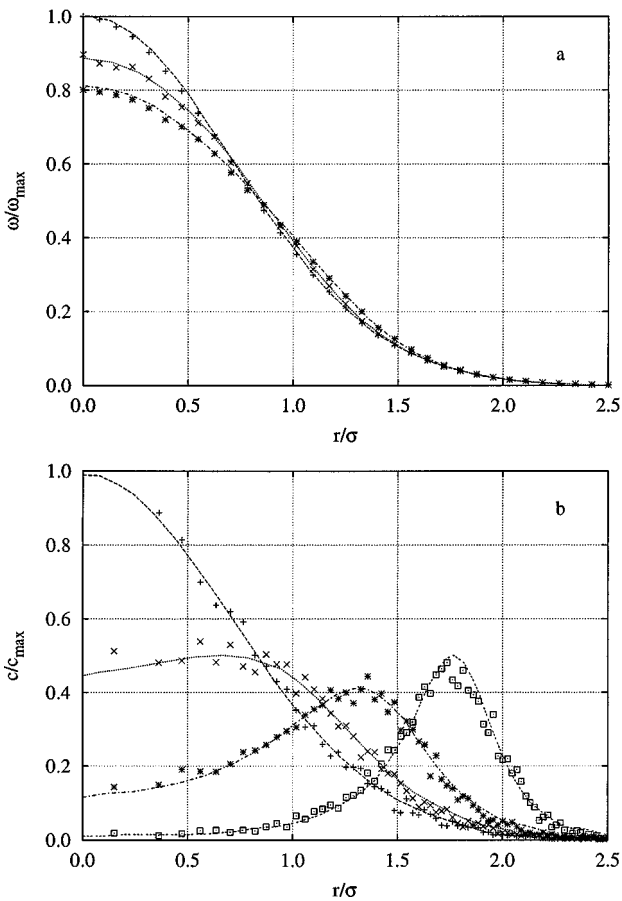

FIG. 4. Vorticity (a) and concentration (b) profiles as function of radius as predicted by the present method (Case 7) at $t = 0$ ($+++$), $t = 20$ ($\times\times\times$), and $t = 60$ ($***$). $t = 140$ ($\square\,\square\,\square$). Lines: finite-difference solution of Chen and Marshall [8].

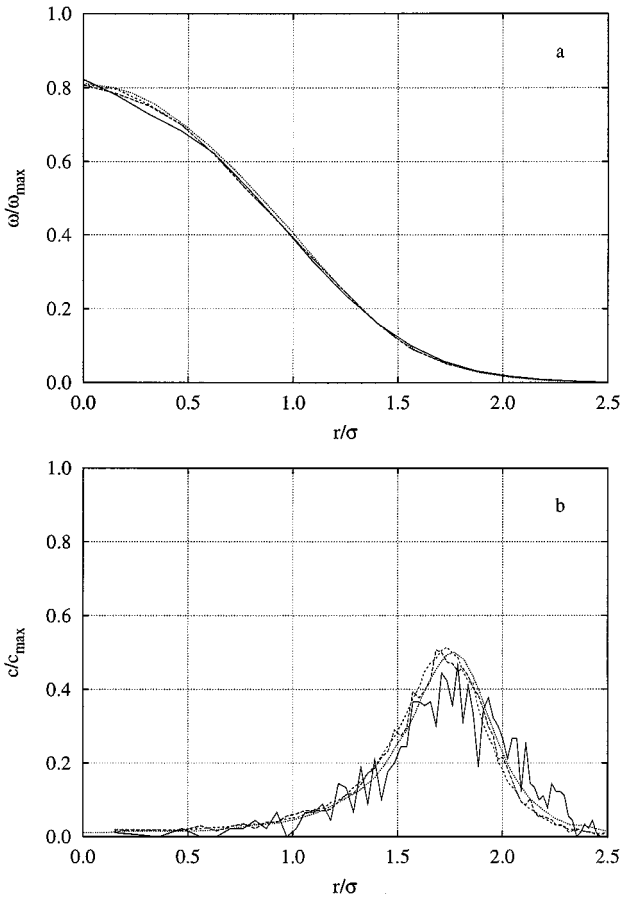

FIG. 5. Vorticity (a) and concentration (b) profile as function of radius for different number of solid particles. Present simulations: —: $N_p = 10^3$ (Case 3); – – –: $N_p = 10^4$ (Case 1); - - -: $N_p = 10^5$ (Case 2). Finite-difference solution of Chen and Marshall [8]: · · ·.

finite-difference solution of Chen and Marshall [8]. Good agreement is observed during the entire simulation (up to $t = 140$).

Next, we study the dependence of the number of solid particles (N_p) on the solution by varying the number of particles two orders of magnitude, $N_p = 10^3$, 10^4, and 10^5, corresponding to 250, 2500, and 25,000 solid particles in two dimensions. The vorticity profiles shown in Fig. 5a are in close agreement with the finite-difference solution (root mean square errors of 1.34%, 0.86%, and 0.75%, respectively) except the case using 10^3 particles, which underestimates the vorticity in the central region of the patch. The concentration profiles (Fig. 5b) exhibit a larger variation than observed in the vorticity but converge to the finite-difference solution as the number of particles is increased (root mean square errors of 6.1%, 2.2%, and 2.8%, respectively). The noise mainly displayed in the concentration profiles (Fig. 5b) is caused by the random initial position of the particles and the inviscid nature of the problem.

The influence of the time step size is demonstrated in Fig. 6 for simulations using a 64^2 mesh and 10^4 particles and for non-dimensional time steps of 0.1 and 0.2. For the parameters investigated a non-dimensional time step of 0.1 appears to be sufficient.

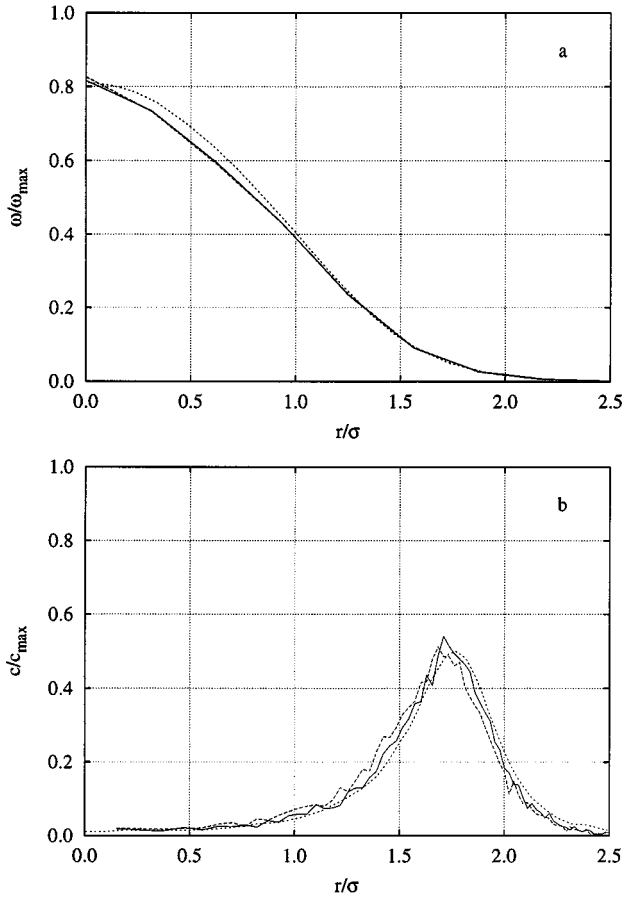

FIG. 6. Vorticity (a) and concentration (b) profile as function of radius for different time step size using a 64^2 mesh and 10^4 particles. Present simulations: —: $\delta t = 0.1$ (Case 4); – – –: $\delta t = 0.2$ (Case 6). Finite-difference solution of Chen and Marshall [8]: - - -.

Finally, the influence of the mesh resolution is studied using 64^2, 128^2, and 256^2 grid points, a time step of 0.1, and 10^4 solid particles, respectively. Good agreement is again observed (Fig. 7) for all but the coarsest mesh, which exhibits some deviations in the vorticity field in the centre of the patch. Thus we conclude that in the parameter range studied the present method produces results in close agreement with those of the high-resolution finite-difference solutions presented in [8].

4.2. *Three-Dimensional Falling "Blob"*

In this section we consider the three-dimensional problem of a suspension of particles initially contained within a spherical boundary and falling due to gravity. The fluid is initially in a quiescent state, without vortex particles, and the test serves to validate the adaptive creation of vortex particles according to the vorticity source term.

The apparent similarity of this problem to that of a viscous drop falling in a fluid has recently been noted by Batchelor and Nitsche [2] in a study of rising bubbles in fluidized beds, and by the same authors [36] for a falling "blob" of particles, where they refer to a "blob" as "a finite volume of a dispersion of particles in a liquid." At low particle Reynolds

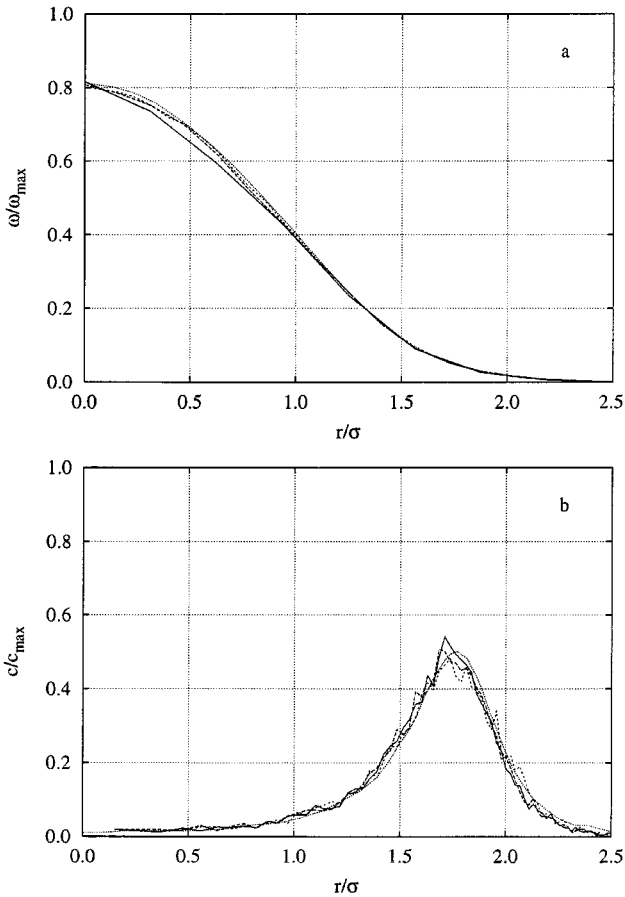

FIG. 7. Vorticity (a) and concentration (b) profile for different mesh resolutions. Present simulations: —: $N_g = 64^2$ (Case 4); – – –: $N_g = 128^2$ (Case 1); - - -: $N_g = 256^2$ (Case 7). Finite-difference solution of Chen and Marshall [8]: · · ·.

numbers ($\mathrm{Re}_p < 1$) they assumed that the particles interact as Stokelets and included an additional short-range repulsive force to regularise the problem. They found that the blob descends faster than a drop of similar density and viscosity and that particles are shed in the wake of the blob by hydrodynamic dispersion. The speed of the blob (u) was compared with the Hadamard and Rybczyński (H–R) formula

$$U = \frac{(\bar{\rho} - \rho) g D^2}{12\mu} \frac{\mu + \bar{\mu}}{\mu + \frac{3}{2}\bar{\mu}}, \tag{27}$$

where $\mu = \rho\nu$ is the dynamic viscosity of the fluid, g is the acceleration due to gravity, and D, $\bar{\mu}$, and $\bar{\rho}$ are the diameter, viscosity, and density of the drop, respectively.

Similar fluid-like behaviour of a suspension has been noted by Powell and Mason [39] in experiments with particle dispersions in laminar shear flows and by Poletto and Joseph [38] in studies of settling spheres in a suspension.

Also, recently Sundaram and Collins [45] used similar arguments in their comparison of particulate flows with pure fluids at an elevated density and viscosity in a study of particle-laden isotropic turbulent flows.

TABLE 2
Numerical Parameters Used in the Study of a Three-Dimensional "Blob" Falling Due to Gravity

Case	N_p	N_g	$\bar{\mu}/\mu$	$\bar{\rho}/\rho$	Re	Fr	u_0/U
1	10^5	$64 \times 64 \times 64$	2.0	2.0	10	0.26	0
2	10^5	$64 \times 64 \times 64$	35.0	1.6	180	1.79	0
3	10^5	$64 \times 64 \times 128$	35.0	1.6	180	1.79	2.3

Note. N_p is the number of solid particles, N_g is the number of grid points, $\bar{\mu}/\mu$ is the viscosity ratio, $\bar{\rho}/\rho$ is the density ratio, u_0/U is the initial velocity, and Re and Fr are the Reynolds and Froude numbers, respectively.

Other numerical studies include the early work of Childress and Peyret [10] on bioconvection using an Eulerian–Lagrangian formulation and the recent study of three-dimensional particle thermals by Li [29].

In the following, we shall compare the speed of a blob with the H–R formula (Eq. (27)) assuming that the density of the blob is given in terms of the (initial) volume fraction (ϕ) as $\bar{\rho} = \rho_p + (1 - \phi)\rho$ and that the viscosity is given by the expression due to Lundgren [30], valid for high-volume fractions,

$$\frac{\bar{\mu}}{\mu} \approx \frac{1}{1 - \frac{5}{2}\phi}. \tag{28}$$

Generally, the parameters governing the flow are the viscosity ratio ($\bar{\mu}/\mu$), the density ratio ($\bar{\rho}/\rho$), the blob Reynolds number $\mathrm{Re} = \rho V D/\mu$, and the Froude number $\mathrm{Fr} = V/\sqrt{gD}$, where V is a characteristic velocity. In the present study we shall use the H–R velocity as the characteristic velocity ($V = U$), reducing the number of parameters to the ratio of viscosity $\bar{\mu}/\mu$, the ratio of density $\bar{\rho}/\rho$, the initial velocity u_0/U, and the Froude number $\mathrm{Fr} = U/\sqrt{gD}$. The results are presented in non-dimensional form based on the diameter of the blob and the H–R velocity.

Three cases are studied. The first case involves a drop falling from rest at moderate Reynolds and Froude numbers ($\mathrm{Re} = 10$ and $\mathrm{Fr} = 0.26$), allowing comparison of the

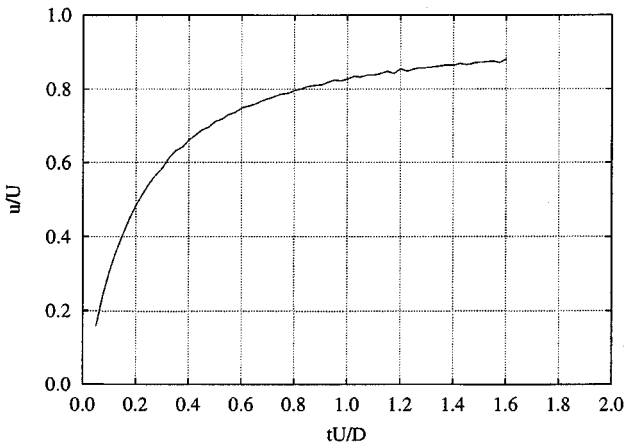

FIG. 8. Speed of the centre of gravity of the suspension (Case 1).

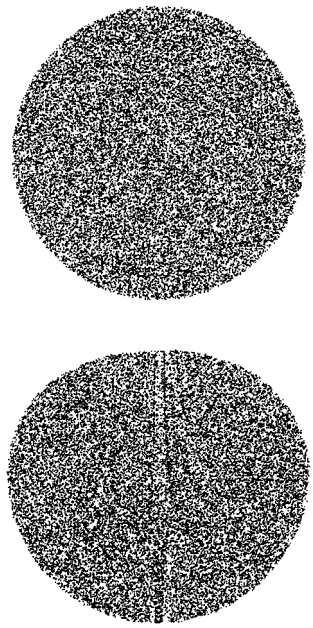

FIG. 9. Cross section of the blob at different non-dimensional times. Top: $tU/D = 0.050$; bottom: $tU/D = 1.325$ (Case 1).

terminal velocity with the H–R formula. The latter two cases involve drops falling at higher Reynolds numbers (Re $= 180$ and 230) matching the viscosity and density ratios at parameters similar to those used by Mitts [34] in studies of falling drops in miscible fluids.

4.2.1. Case 1. The first simulation involves a drop falling from rest at Reynolds number Re $= 10$, and Froude number of Fr $= 0.26$. At this relatively low Reynolds number we

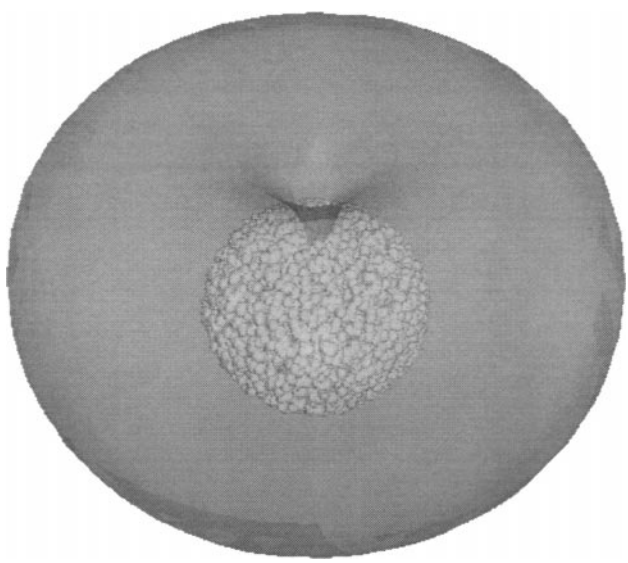

FIG. 10. Iso-surface of vorticity ($|\omega|/|\omega_{\max}| = 0.1$) and one-tenth of the solid particles at $tU/D = 1.325$ (Case 1).

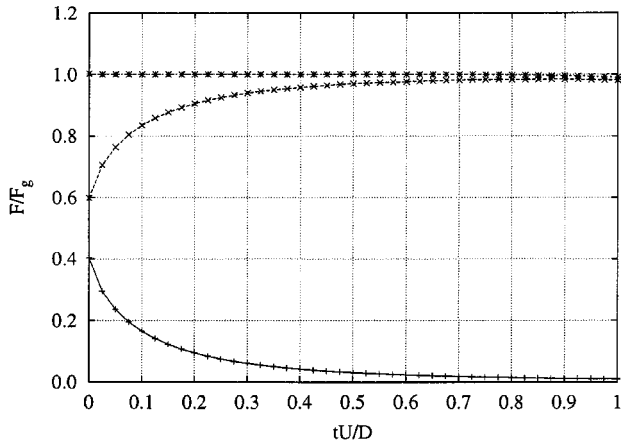

FIG. 11. Total force on the particular and fluid phase. $-\times-\times-$: total fluid force; $-+-+-$: total solid particle force; $-*-*-$: total force on system.

expect that the terminal velocity of the blob can be compared with the H–R velocity. The viscosity and density ratios are $\bar{\mu}/\mu = \bar{\rho}/\rho = 2$. The drop is modelled by placing 10^5 solid particles within a spherical boundary of diameter D and the size of the computational domain is $(10D \times 10D \times 10D)$ discretised using 64^3 grid points. The parameters are summarised in Table 2.

The time history of the non-dimensional speed of the centre of gravity of the blob is shown in Fig. 8. The estimated limiting value of u/U is 0.89, thus in fair agreement with the H–R formula considering the approximations involved. A cross section of the blob at $tU/D = 0.050$ and $tU/D = 1.325$ is shown in Fig. 9. At this finite Reynolds number, the blob deforms during the descent, but remains intact in the time span studied. The corresponding vorticity field and one-half of the solid particles are shown in Fig. 10 at $tU/D = 1.325$. The blob has created a vortex ring that propagates with the blob.

The conservation of momentum between the phases is demonstrated by considering the time history of the total vertical force acting on the solid particles ($F = \sum f_d + f_g$) and

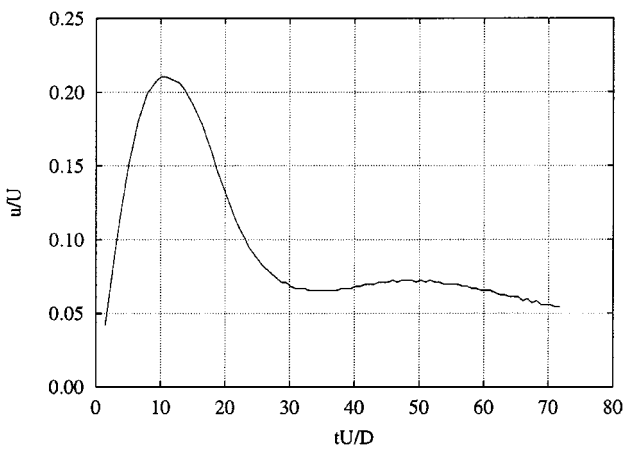

FIG. 12. Speed of the centre of gravity of the suspension (Case 2).

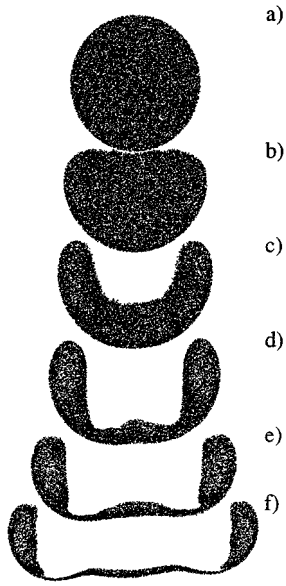

FIG. 13. Cross section of the blob at different non-dimensional times (tU/D). (a) 0.00, (b) 7.18, (c) 10.77, (d) 14.36, (e) 17.94, and (f) 21.53.

the total fluid forces ($-\sum f_d$) normalised by the total gravitational force ($F_g = \sum f_g$) on the solid particles as shown in Fig. 11. The total force on the solid particles is evaluated from the rate of change of the particle momentum as $\sum d(mv_p)/dt$, and the fluid force is computed from Eq. (22). The total force on the solid particles decreases monotonically

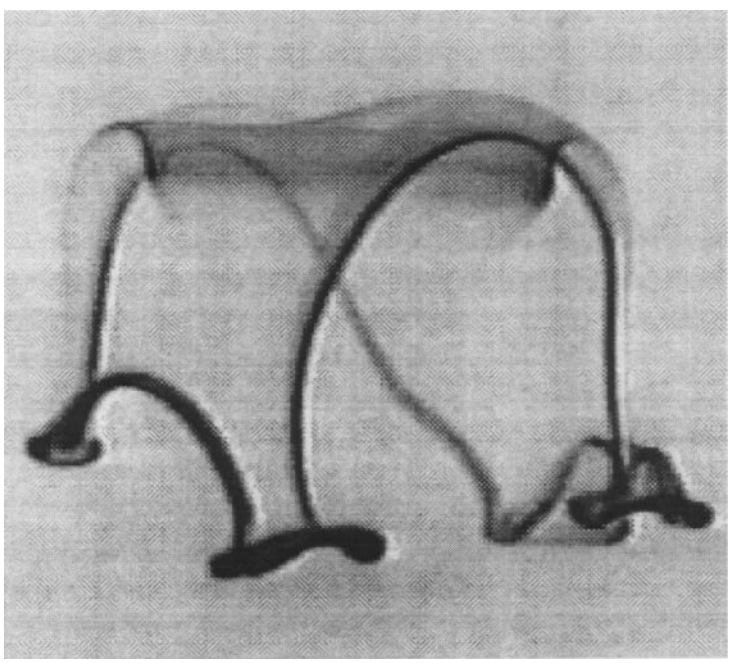

FIG. 14. Picture of experimental results from Mitts [34].

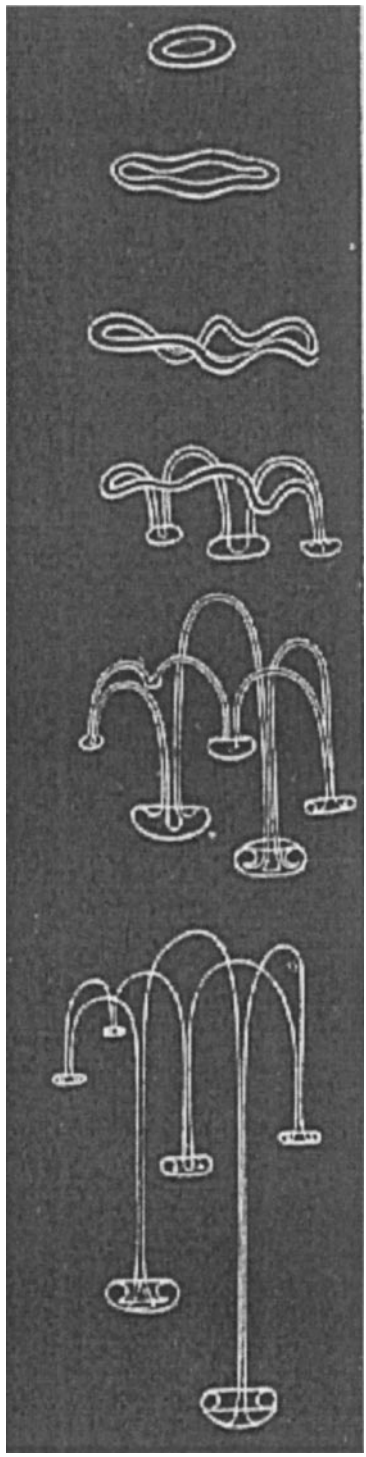

FIG. 15. Sketch of unstable vortex ring from experiments by Thomson and Newall [48].

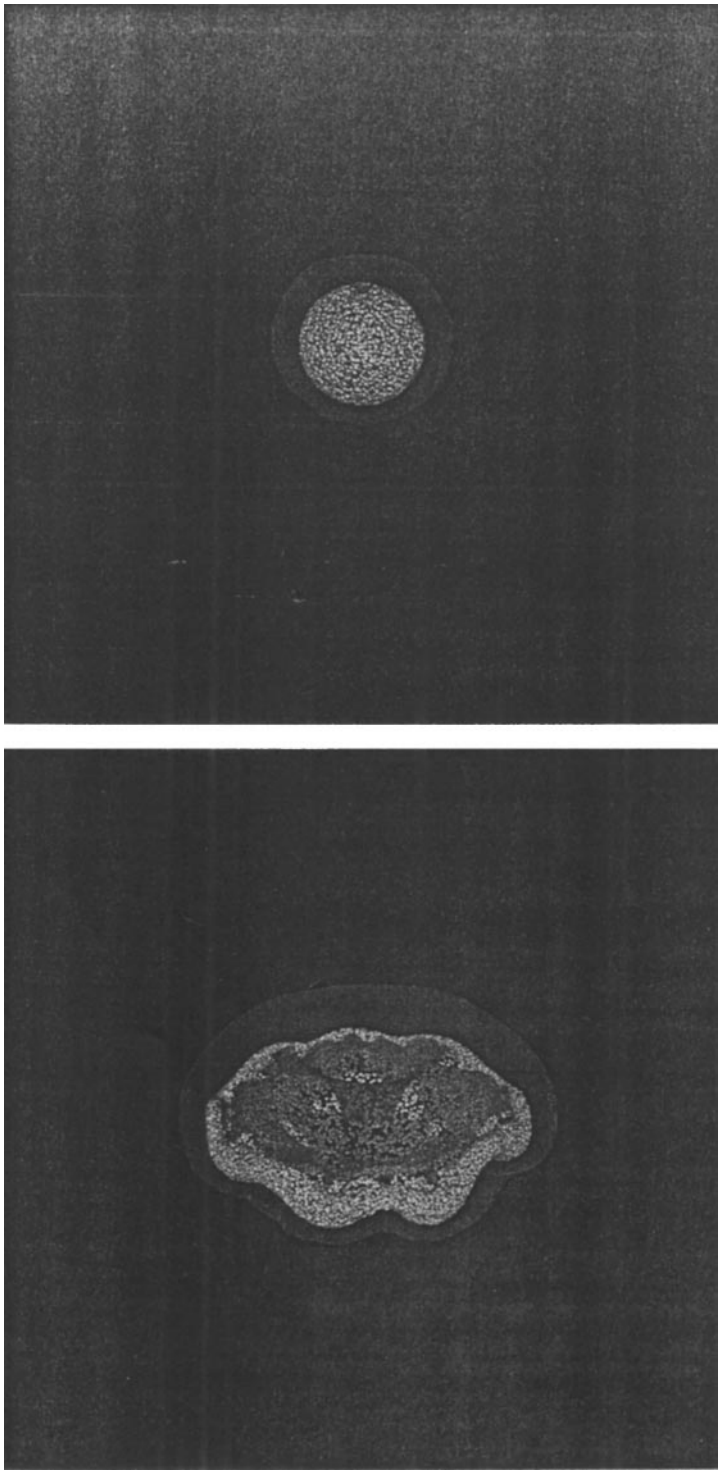

FIG. 16. Vorticity iso-surfaces (red, $|\omega|/|\omega_{\max}| = 0.12$) and solid particles (1/2 of total) at different non-dimensional time (Case 2). From the top $tU/D = 3.59$, 35.9, 53.8, 71.8, and 171.5.

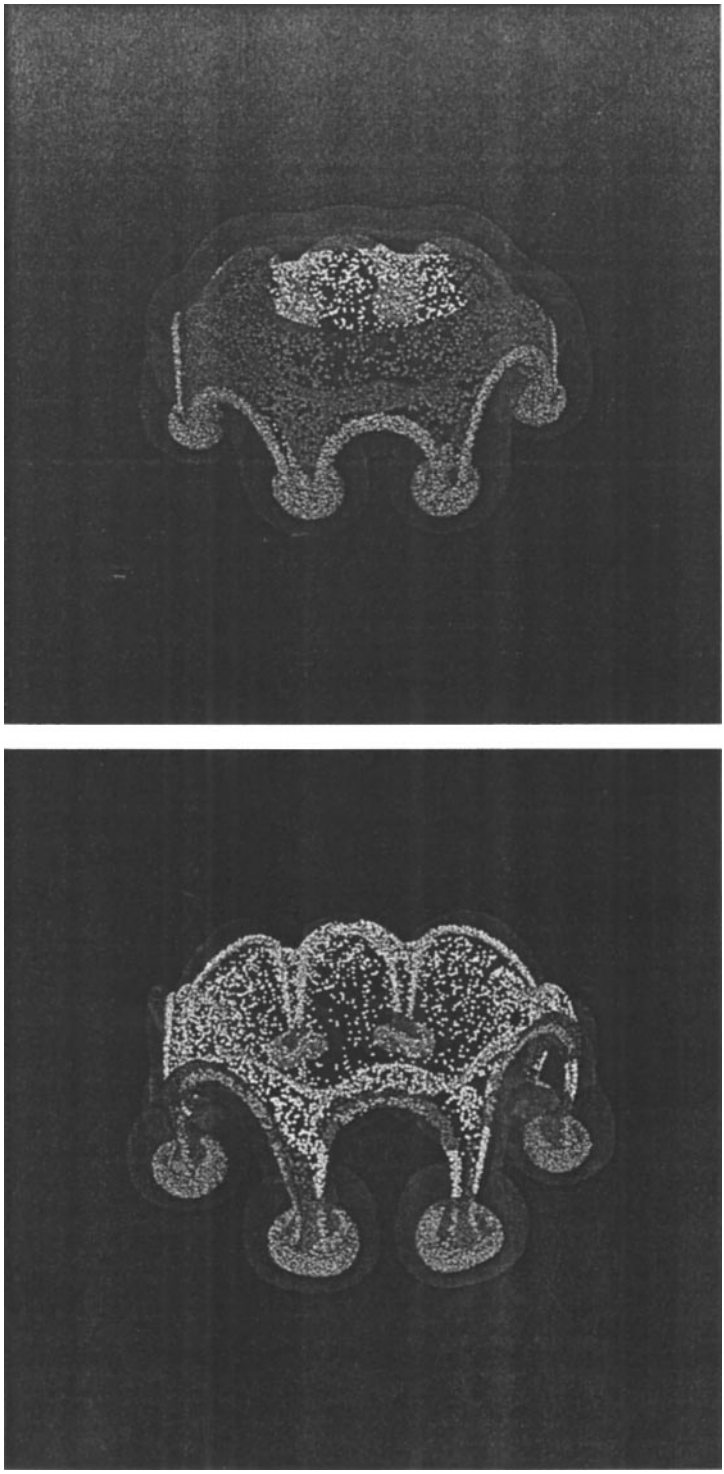

FIG. 16—*Continued*

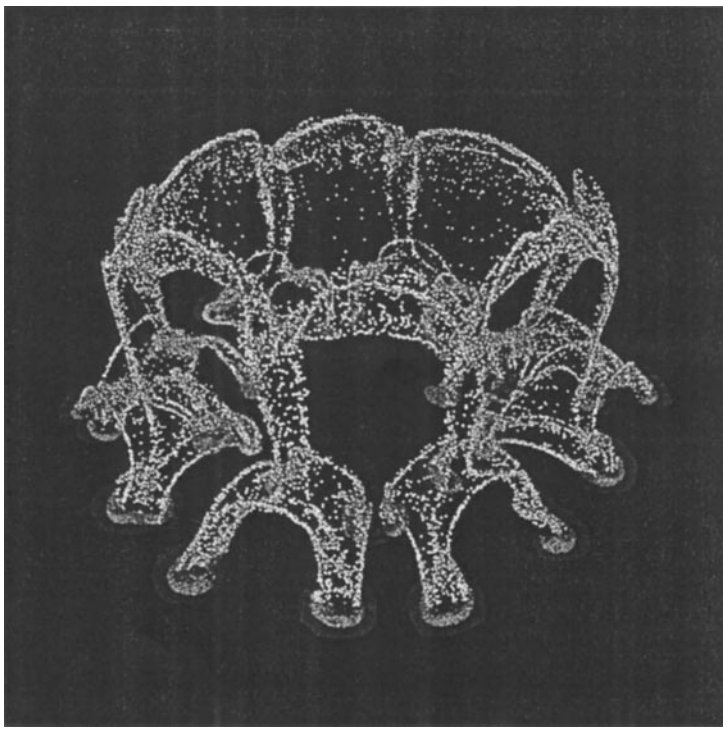

FIG. 16—*Continued*

towards zero (as drag is being balanced by gravity) and the fluid force increases correspondingly. For the duration of the simulation the momentum is clearly conserved.

4.2.2. Case 2. The second case involves a highly viscous drop ($\bar{\mu}/\mu = 35$) falling at a Reynolds number of 180 and Froude number of 1.79, respectively. The density ratio is $\bar{\rho}/\rho = 1.6$. The parameter values are similar to the values used in the experiments of viscous drops falling in a miscible fluid by Mitts [34]. In these experiments the drops were formed above the bath and allowed to fall some distance before penetrating the surface of the bath. Thus the simulations differ from the experiments in terms of initial conditions.

The speed of the centre of gravity of the blob computed with the present method is shown in Fig. 12. It is observed that the blob accelerates from rest until it reaches a maximum speed of approximately one-fifth of the H–R speed, followed by a deceleration to a mean value of approximately $\frac{1}{15}$ of the H–R value. The cause of the deceleration can be inferred from snapshots of the cross section of the blob as shown in Fig. 13. As the blob descends it deforms from the initial spherical shape into an oblate spheroid due to the resistance exerted by the fluid. An intrusion develops at the rear stagnation point and the blob subsequently forms into a spherical cap shape as shown in Fig. 13c. As the blob expands the drag force increases, hence retarding the blob. At later times, the blob transforms into an unstable ring. Bulges form along the ring, and these form new blobs that descend faster than the main ring. After traveling some distance these blobs again form new rings in a cascade-like fashion. Similar observations were made in the experiments by Mitts [34] (cf. Fig. 14) and sketched in the work of Thomson and Newall [48] (Fig. 15). The solid particles and the iso-surface of vorticity ($|\omega|/|\omega_{\max}| = 0.08$) are shown in Fig. 16. The particles are indicated with

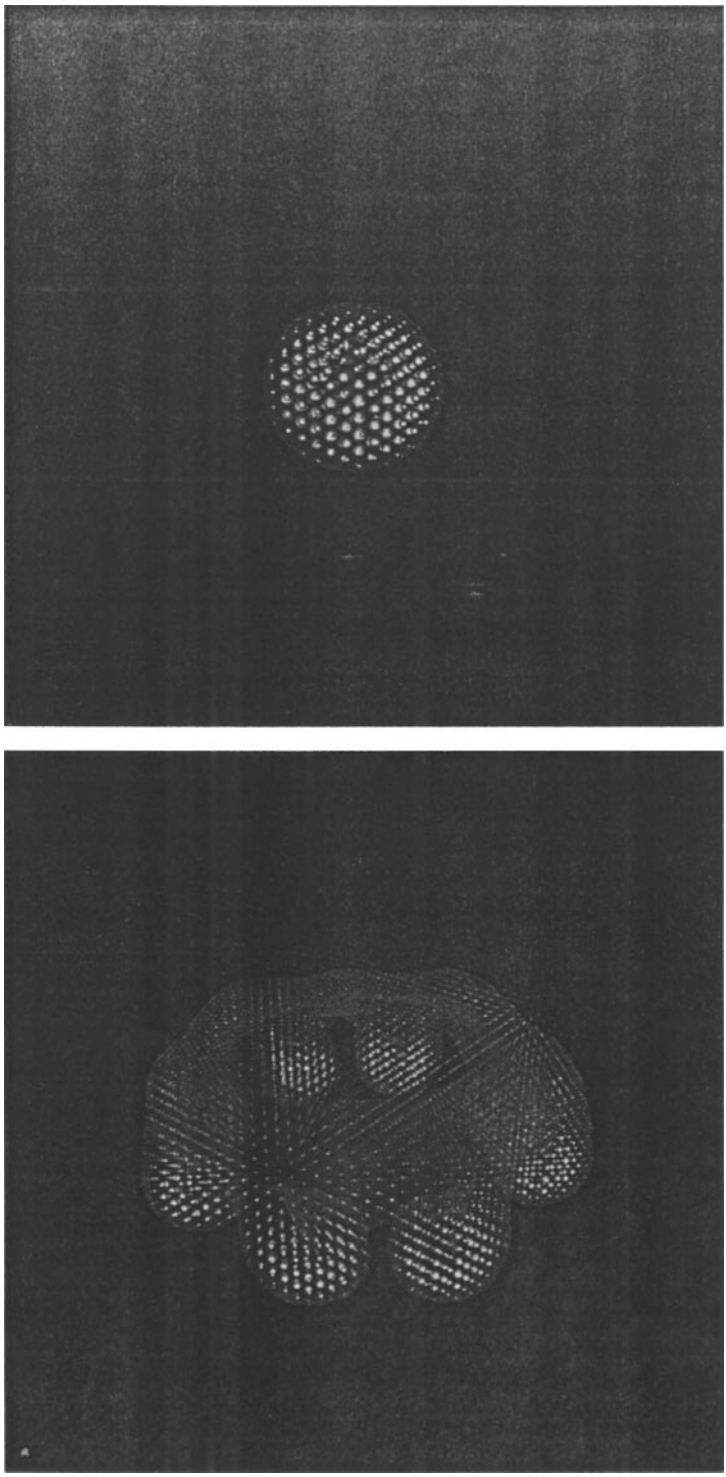

FIG. 17. Vorticity iso-surfaces (red) and the vortex particles (Case 2). Top: $tU/D = 3.59$; bottom: $tU/D = 53.8$.

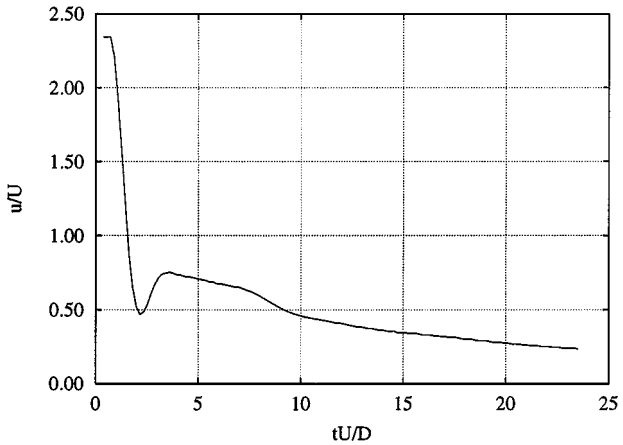

FIG. 18. Speed of the centre of gravity of the suspension (Case 3).

white spheres and partially covered by the transparent iso-surface shown in red. The vortex particle support is shown in Fig. 17, where the vortex elements are plotted as spheres with a diameter proportional to their strength. The figure clearly demonstrates the adaptivity of the method.

4.2.3. Case 3. This last test case involves a blob with physical properties identical to those in the previous case (Case 2), but for this study the blob is allowed to fall some distance with a constant velocity, creating fluid vorticity, before it is "released" into the flow. This

FIG. 19. Cross section of the blob at different non-dimensional times (tU/D) (Case 3). (a) 0.03, (b) 0.75, (c) 1.47, (d) 2.91, (e) 7.21, and (f) 21.57.

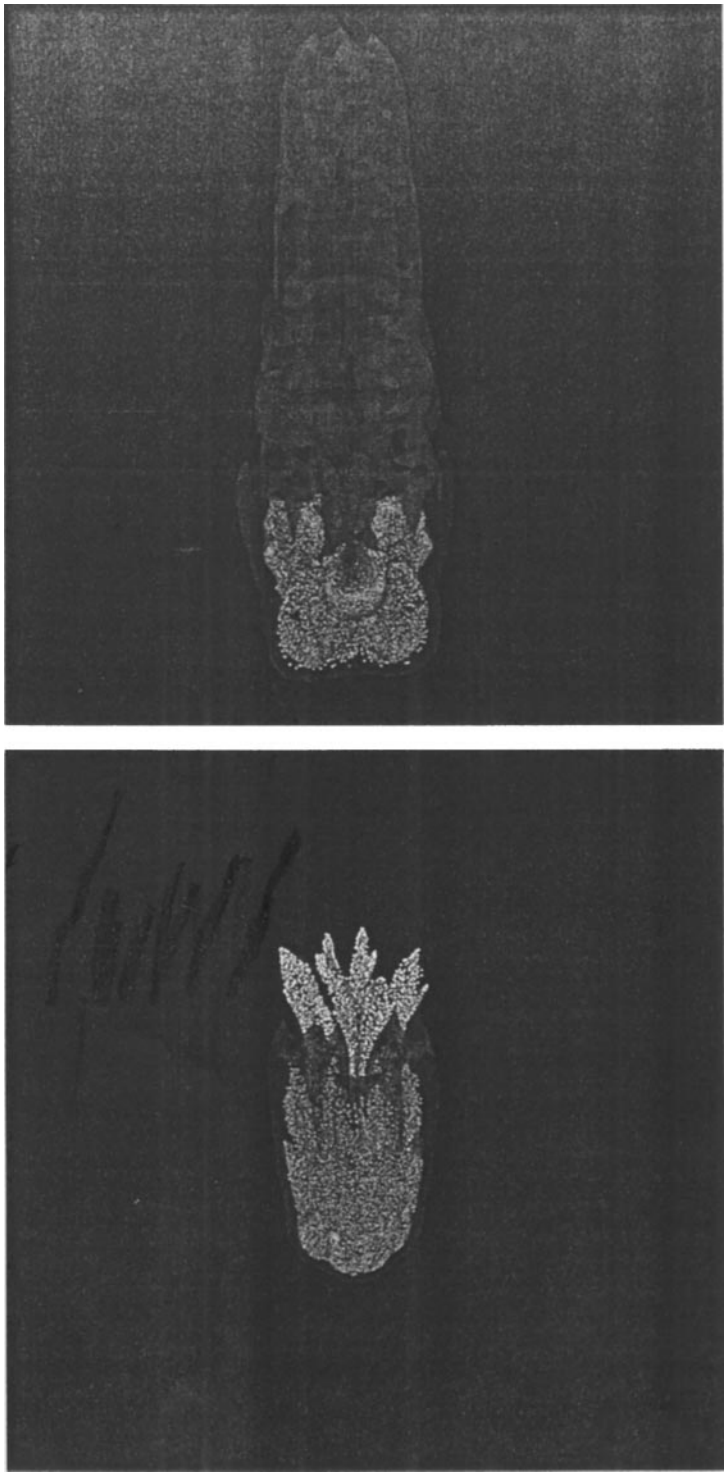

FIG. 20. Vorticity iso-surfaces (red) and solid particles (1/2 of total) at different non-dimensional times (Case 3.) From the top: $tU/D = 3.59, 7.18, 10.77, 14.36, 17.94$, and 21.53.

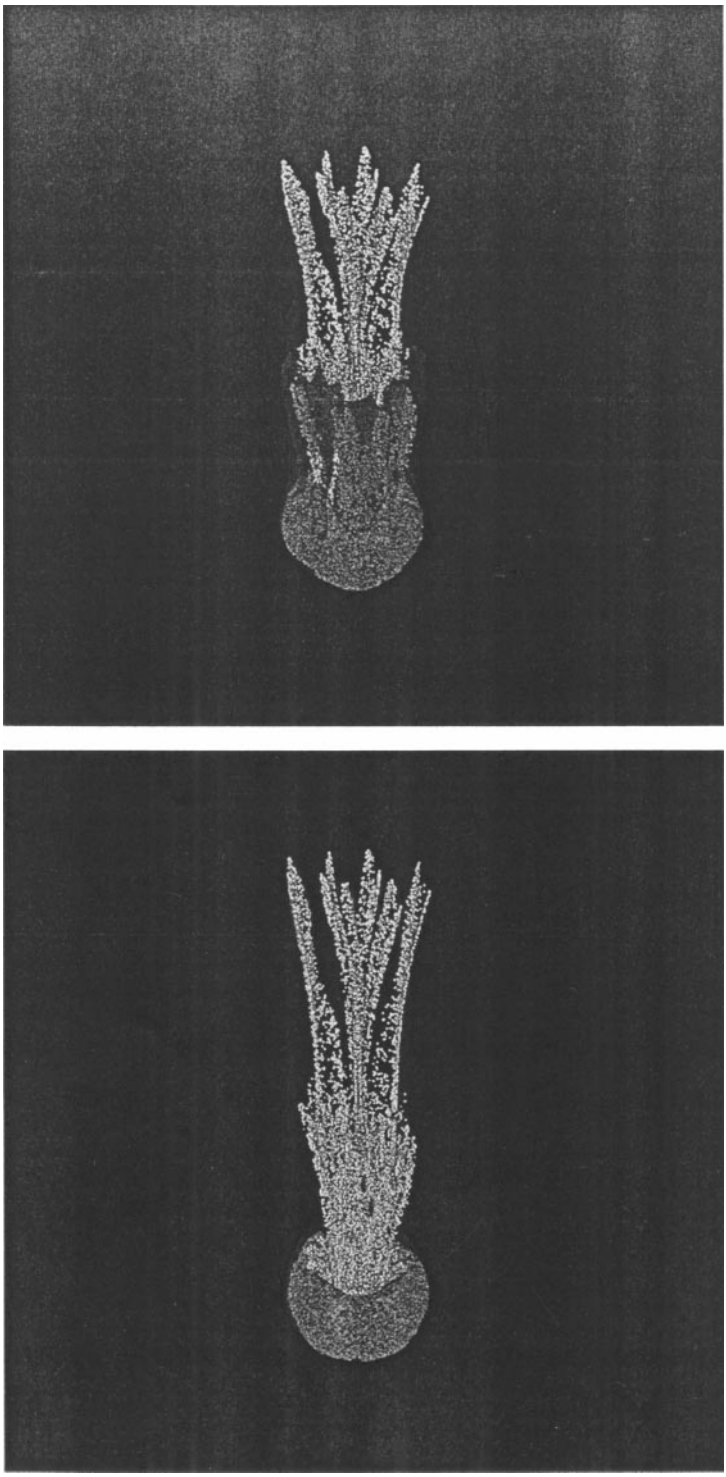

FIG. 20—*Continued*

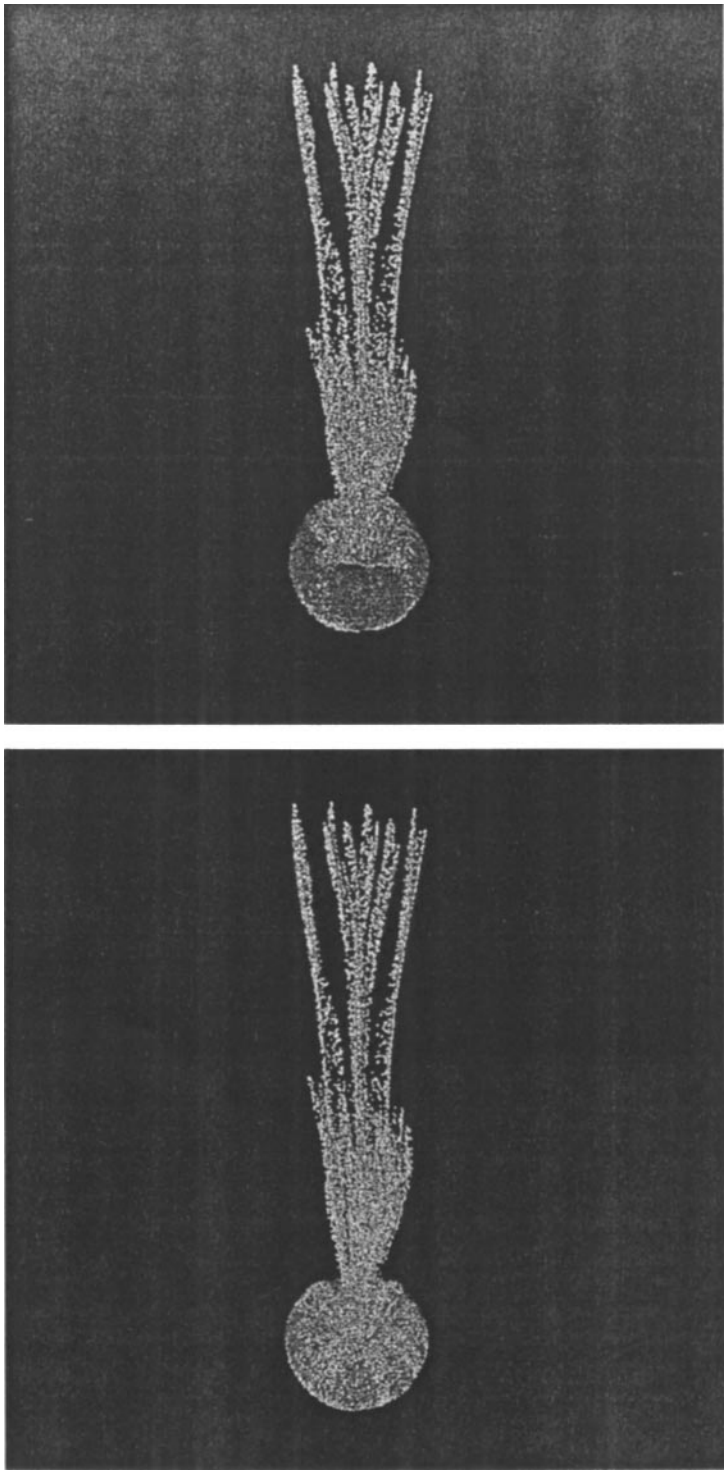

FIG. 20—*Continued*

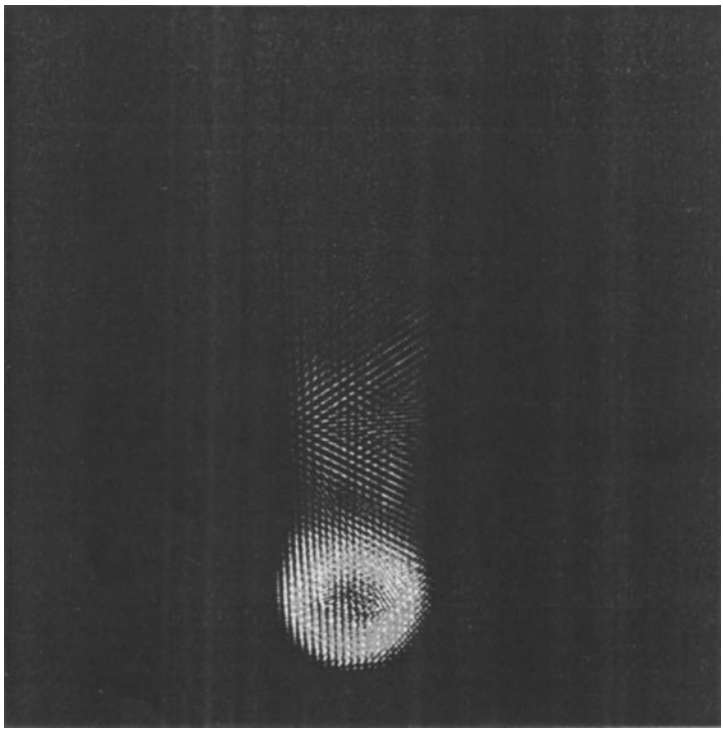

FIG. 21. Vorticity iso-surfaces (red) and the vortex particles (Case 3) at $tU/D = 21.53$.

effective one-way coupling of the phases is similar to the model proposed by Thomson and Newall [48] for the formation of a vortex ring from a drop falling into a bath.

The time history of the speed of the drop is shown in Fig. 18. As the drop is released at $tU/D = 0.72$ the speed decreases from the initial value of 2.3 to a value of 0.5 followed by a temporary increase to approximately 0.75, after which the speed decreases monotonically. The initial deceleration is attributed to an expansion of the blob as shown in Figs. 19a–19c. The blob transforms into a ring at $tU/D \approx 8$, but with a loss of particles shed in the wake; cf. Fig. 19f. The increase in speed of the centre of gravity at $tU/D \approx 2.5$ is due to a strong reorganisation of the particles, cf. Figs. 19d, 19e. Similar observations were noted in a study of vortex rings by Mansfield *et al.* [31].

The iso-surface of the vorticity ($|\omega|/|\omega_{\max}| = 0.02$) and the solid particles are shown in Fig. 20. The initial "rigid" drop introduces an intense wake which remains for some time contrary to the previous case where the vorticity more closely follows the drop. The corresponding vortex particles supporting the vorticity field are shown in Fig. 21.

5. CONCLUSIONS

A three-dimensional vortex particle method has been developed for the study of two-phase particulate flows with two-way coupling. The method employs a Lagrangian procedure for motion of the solid particles and utilises well established formulas for the hydrodynamic forces acting on solid particles. The fluid flow is solved using an adaptive particle method based on an enhanced vortex-in-cell algorithm. The individual fluid elements carrying

vorticity evolve subject to convection, stretching, and diffusion, and change due to the vorticity source term determined from the rotational part of the forcing induced by the solid particles. An adequate particle support for this source term is secured by a re-meshing strategy which combines the forcing term with projection of the Lagrangian fluid elements onto a regular grid. The projection uses high-order, moment-conserving spline formulas, hence minimising spurious forcing of the flow. The re-meshing procedure allows the adaptive creation of vortex elements in the regions of the flow where the local vorticity is non-negligible.

The Lagrangian procedure adopted for the fluid flow avoids the discretisation of the non-linear term making this methods an interesting alternative to traditional grid based methods.

The method is validated by the simulation of a suspension of solid particles embedded in an inviscid, two-dimensional patch of vorticity. The results are found to be in good agreement with previous benchmark calculations. The features of the proposed method are further investigated through the study of an initially spherical suspension of particles falling due to gravity in a quiescent viscous fluid. At low Reynolds numbers the suspension forms a steady vortex ring travelling with the suspension. The speed of the ring is found in resonable agreement with the classical Hadamard and Rybczyński velocity for a drop falling in a viscous fluid.

For higher Reynolds and Froude numbers the vortex ring is unstable, forming bulges along its circumference. As these bulges descend new vortex rings are created in a cascade-like fashion and in qualitative agreement with experimental observations of drops falling in a viscous fluid, cf. Thompson [47]. The instability was found to depend on the initial vorticity field, and further studies are under way to quantify this dependence.

ACKNOWLEDGMENT

We acknowledge many helpful discussions with Professor G.-H. Cottet. We have benefited from many discussions with Professor D. Poulikakos, who introduced us to the problem of falling drops.

REFERENCES

1. Gregory R. Baker, Daniel I. Meiron, and Steven A. Orszag, Vortex simulations of the Rayleigh–Taylor instability, *Phys. Fluids* **23**(8), 1485 (1980).
2. G. K. Batchelor and J. M. Nitsche, Expulsion of particles from a buoyant blob in a fludized bed, *J. Fluid Mech.* **278**, 63 (1994).
3. J. Thomas Beale and Andrew Majda, Vortex methods. II. Higher order accuracy in two and three dimensions, *Math. Comput.* **39**(159), 29 (1982).
4. Charles K. Birdsall and Dieter Fuss, Clouds-in-clouds, clouds-in-cells physics for many-body plasma simulation, *J. Comput. Phys.* **3**, 494 (1969).
5. Stephen G. Brecht and John R. Ferrante, Vortex-in-cell calculations in three dimensions, *Comput. Phys. Commun.* **58**, 25 (1990).
6. Stephen H. Brecht and John R. Ferrante, Vortex-in-cell simulation of buoyant bubbles in three dimensions, *Phys. Fluids A* **1**(7), 1166 (1989).
7. Reiyu Chein and J. N. Chung, Simulation of particle dispersion in a two-dimensional mixing layer, *AIChe J.* **34**(6), 946 (1998).
8. H. Chen and J. S. Marshall, A Lagrangian vorticity method for two-phase particulate flows with two-way phase coupling, *J. Comput. Phys.* **148**, 169 (1999).
9. H. Cheng, L. Greengard, and V. Rokhlin, A fast adaptive multipole algorithm in three dimensions, *J. Comput. Phys.* **155**, 468 (1999).

10. S. Childress and R. Peyret, A numerical study of two-dimensional convection by motile particles, *J. Mec.* **15**(5), 753 (1976).
11. Alexandre Joel Chorin, Hairpin removal in vortex interactions, *J. Comput. Phys.* **91**(1), 1 (1990).
12. J. P. Christiansen, Numerical simulation of hydrodynamics by the method of point vortices, *J. Comput. Phys.* **13**, 363 (1973).
13. G.-H. Cottet, artifical viscosity models for vortex and particle methods, *J. Comput. Phys.* **127**, 299 (1996).
14. G.-H. Cottet, Personal communication, 1999.
15. G.-H. Cottet and P. Koumoutsakos, *Vortex Methods: Theory and Practice* (Cambridge Univ. Press, New York, 2000).
16. C. T. Crowe, T. R. Troutt, and J. N. Chung, Numerical models for two-phase turbulent flows, *Annu. Rev. Fluid Mech.* **28**, 11 (1996).
17. P. Degond and S. Mas-Gallic, The weighted particle method for convection-diffusion equations. 1. The case of an isotropic viscosity, *Math. Comput.* **53**(188), 485 (1989).
18. J. K. Eaton and J. R. Fessler, Preferential concentration of particles by turbulence, *Int. J. Multiphase Flow.* **20**(Suppl), 169 (1994).
19. R. P. Feynman, Application of quantum mechanics to liquid helium, *Prog. Low Temp. Phys.* **1**, 17 (1955).
20. C. A. J. Fletcher, *Computational Techniques for Fluid Dynamics. Fundamental and General Techniques*. 2nd ed. I (Springer-Verlag, Berlin/New York, 1991), Vol. I.
21. Roland Glowinski, Tsorng-Whay Pan, Todd I. Hesla, Daniel D. Joseph, and Jacques Periaux, A distributed Lagrange multiplier/fictitious domain method for flows aound moving rigid bodies: Application to particulate flow, *Int. J. Numer. Methods Fluids* **30**, 1043 (1999).
22. Ole H. Hald, Convergence of vortex methods for Euler's equations, II, *SIAM J. Numer. Anal.* **16**(5), 726 (1979).
23. R. W. Hockney and J. W. Eastwood, *Computer Simulation Using Particles*, 2nd ed. (IOP, 1988).
24. J. C. R. Hunt, Industrial and environmental fluid mechanics, *Annu. Rev. Fluid Mech.* **23**, 1 (1991).
25. Robert M. Kerr, Simulation of Rayleigh–Taylor flows using vortex blobs, *J. Comput. Phys.* **76**, 48 (1988).
26. Omar M. Knio and Ahmed F. Ghoniem, Three-dimensional vortex simulation of rollup and entranment in a shear layer, *J. Comput. Phys.* **97**, 172 (1991).
27. P. Koumoutsakos, Inviscid axisymmetrization of an elliptical vortex ring, *J. Comput. Phys.* **138**, 821 (1997).
28. A. Leonard, Vortex methods for flow simulations, *J. Comput. Phys.* **37**, 289 (1980).
29. C. W. Li, Convection of particle thermals (convection de nuages de particules), *J. Mec.* **35**(3), 363 (1997).
30. T. S. Lundgren, Slow flow through stationary random beads and suspensions of spheres, *J. Fluid Mech.* **51**(2), 273 (1972).
31. John R. Mansfield, Omar M. Knio, and Charles Meneveau, Dynamics LES of colliding vortex rings using a 3Df vortex method, *J. Comput. Phys.* **152**, 305 (1999).
32. J. E. Martin and E. Meiburg, The accumulation and dispersion of heavy particles in forced two-dimensional mixing layers. I. The fundamental an subharmonic cases, *Phys. Fluids* **6**(3), 1116 (1994).
33. M. R. Maxey and J. J. Riley, Equation of motion for a small rigid sphere in a non-uniform flow, *Phys. Fluids A* **26**, 883 (1983).
34. Chad J. Mitts, *An Investigation of Transcritical Droplet Dynamics through the Use of a Miscible Fluid Analog*, Ph.D. Thesis (University of Illinois at Chicago, 1996).
35. J. J. Monaghan, Extrapolating B splines for interpolation, *J. Comput. Phys.* **200**, 253 (1985).
36. J. M. Nitsche and G. K. Batchelor, Break-up of a falling drop containing dispersed particles, *J. Fluid Mech.* **340**, 161 (1997).
37. C. W. Oseen, *Neuere Methoden und Ergebnisse in der Hydrodynamik* (Akad. Verlagsgesellshaft, Leipzig, 1927).
38. Massimo Poletto and Daniel D. Joseph, Effective density an viscosity of a suspension, *J. Rheol.* **39**(2), 323 (1995).
39. R. L. Powell and S. G. Mason, Dispersion by laminar flow, *AIChe J.* **28**(2), 286 (1982).

40. P. A. Raviart, *An Analysis of Particle Methods*, Lecture Notes in Mathematics (Springer-Verlag, Berlin, 1983), Vol. 1127, p. 243.
41. P. G. Saffman, *Vortex Dynamics* (Cambridge Univ. Press, Cambridge, UK, 1992).
42. J. T. Sagredo, J. H. Walther, and P. Koumoutsakos, High resolution vortex-in-cell methods, submitted for publication.
43. Green Mountain Software, *Crayfishpak. User's Guide* (Madeira Beach, FL, 1990).
44. Shivshankar Sundaram and Lance R. Collins, Numerical considerations in simulating a turbulent suspension of finite-volume particles, *J. Comput. Phys.* **124**, 337 (1996).
45. Shivshankar Sundaram and Lance R. Collins, A numerical study of the modulation of isotropic turbulence by suspended particles, *J. Fluid Mech.* **379**, 105 (1999).
46. L. Tang, F. Wen, Y. Yang, C. T. Crowe, J. N. Chung, and T. R. Troutt, Self-organizing particle dispersion mechanisms in a plane wake, *Phys. Fluids A* **4**, 2244 (1992).
47. D'Arcy Wentworth Thompson, *On Growth and Form* (Dover, New York, 1992).
48. J. J. Thomson and H. F. Newall, On the formation of vortex rings by drops falling into liquids, and some allied phenomena, *Proc. R. Soc.* **39**, 417 (1885).
49. Grétar Tryggvason, Numerical simulations of the Rayleigh-Taylor instability, *J. Comput. Phys.* **75**, 253 (1988).
50. J. H. Williamson, Low-storage runge-kutta schemes, *J. Comput. Phys.* **35**, 48 (1980).
51. Juan A. Zufiria, Vortex-in-cell simulation of bubble competition in Rayleigh–Taylor instability, *Phys. Fluids*, **31**(11), 3199 (1988).
52. Juan A. Zufiria, Linear analysis of the vortex-in-cell algorithm applied to Rayleigh–Taylor instability, *J. Comput. Phys.* **80**, 387 (1989).